RESEARCH ARTICLE

A polarization-sensitive, self-powered, broadband and fast $Ti_3C_2T_x$ MXene photodetector from visible to near-infrared driven by photogalvanic effects

Bo Liu, Liyu Qian, Yanliang Zhao, Yiwen Zhang, Feng Liu, Yi Zhang†, Yiqun Xie‡, Wangzhou Shi

Department of physics, Shanghai Normal University, Shanghai 200234, China
Corresponding authors. E-mail: †yzhang@shnu.edu.cn, ‡yqxie@shnu.edu.cn

Supporting Information

Experimental section

Figure S1 gives AFM results and size distribution for few-layer $Ti_3C_2T_x$ MXene. Figure S2 shows XPS results. Polarization dependent current of the four devices along the *x*- and *y*-directions at 1064 nm are given in Figs. S3 and S4. We have also examined the repeatability of the Device-8 as an example, as shown in Fig. S5. The sample is irradiated by the time-dependent periodic laser light (1064 nm) for 6000 seconds, during which the magnitude of the photocurrent is almost invariant with a reduction less than 1%，indicating a good repeatability.

.

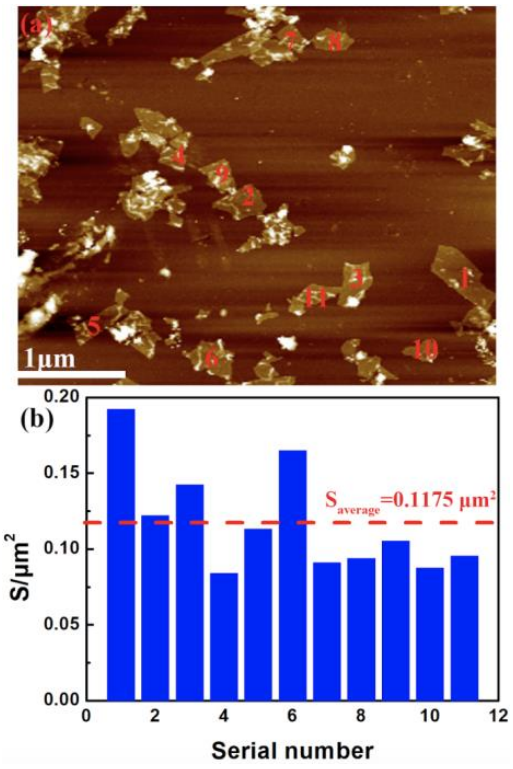

Fig. S1 (a) Few-layer $Ti_3C_2T_x$ MXene AFM results, **(b)** size distribution.

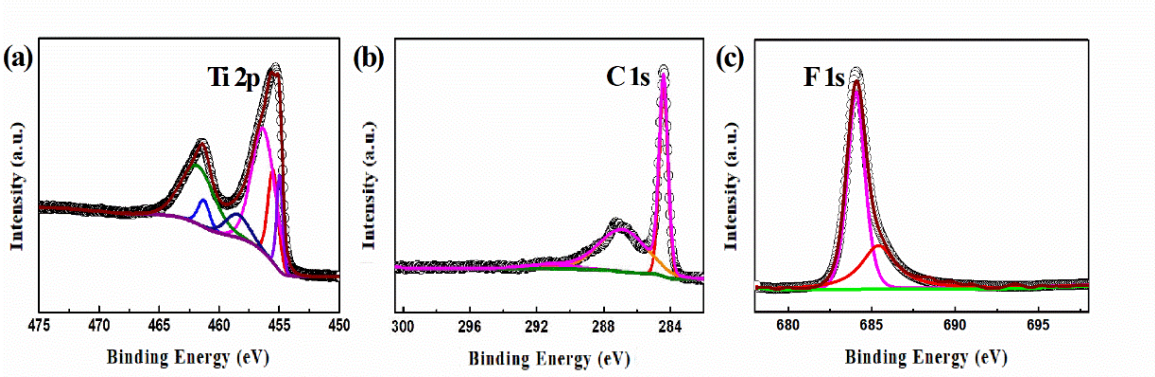

Fig. S2 Fitting results of Ti 2p **(a)** C 1s **(b)** and F 1s **(c)** of XPS.

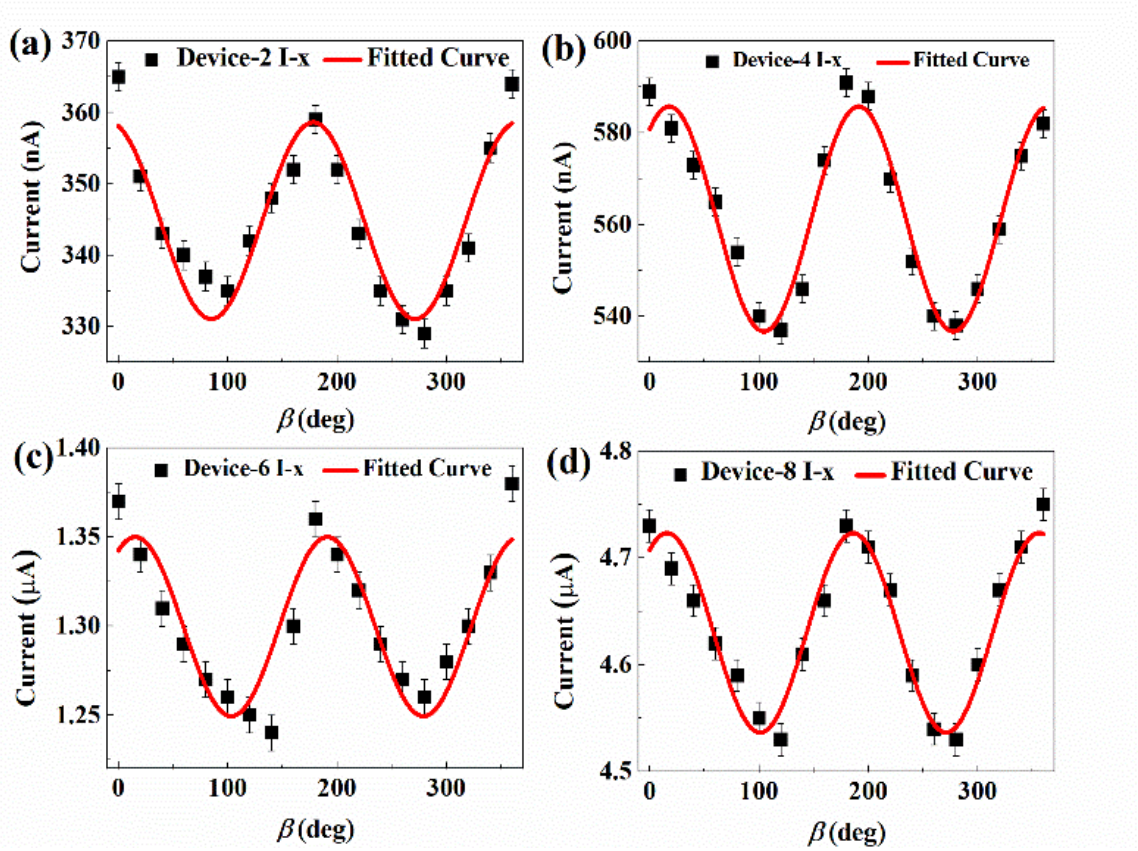

Fig. S3 Polarization dependent current of the four devices along the *x*-direction at 1064 nm.

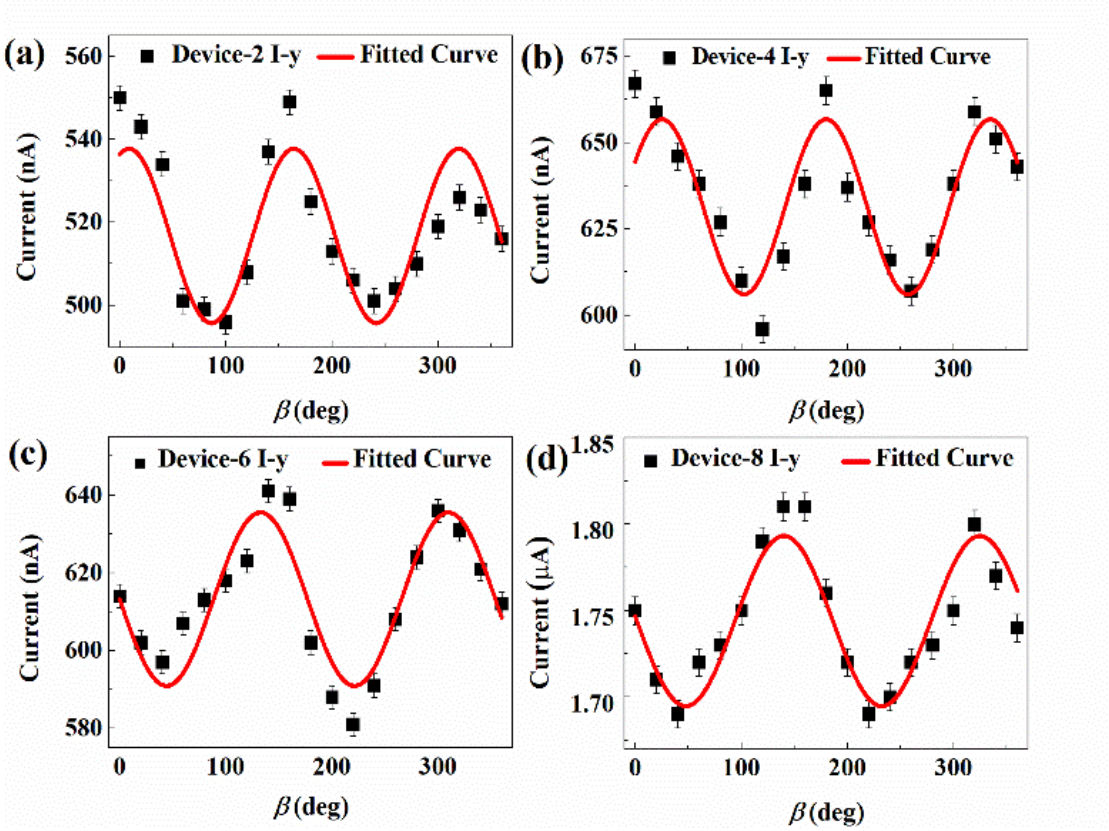

Fig. S4 Polarization dependent current of the four devices along the *y*-direction at 1064 nm.

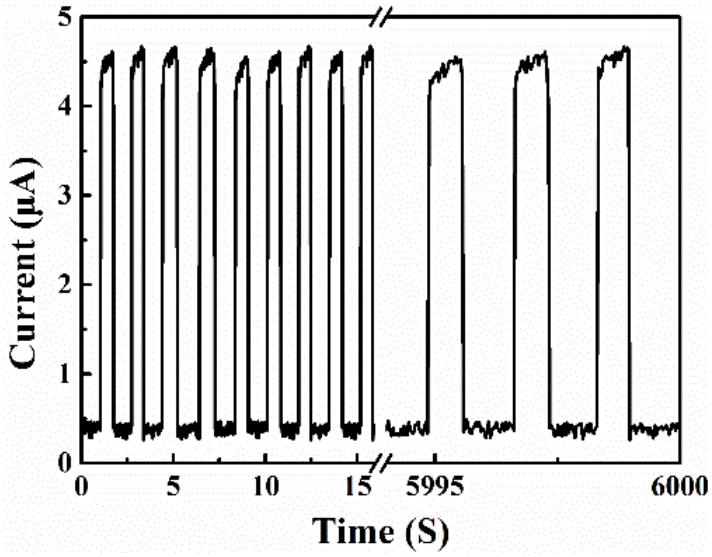

Fig. S5 Time-dependent curve of Device-8 under 1064 nm laser.

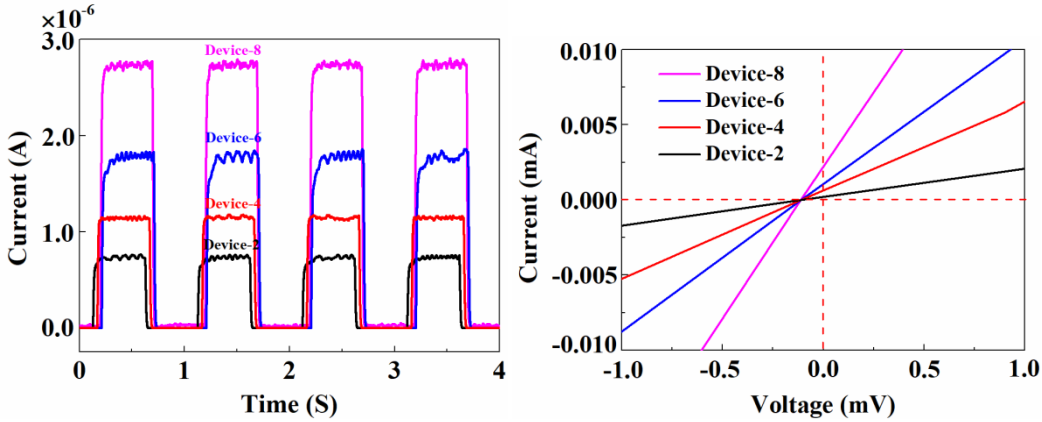

Fig. S6 *I-T* and *I-V* characteristic curves of samples prepared with NMP solvent.

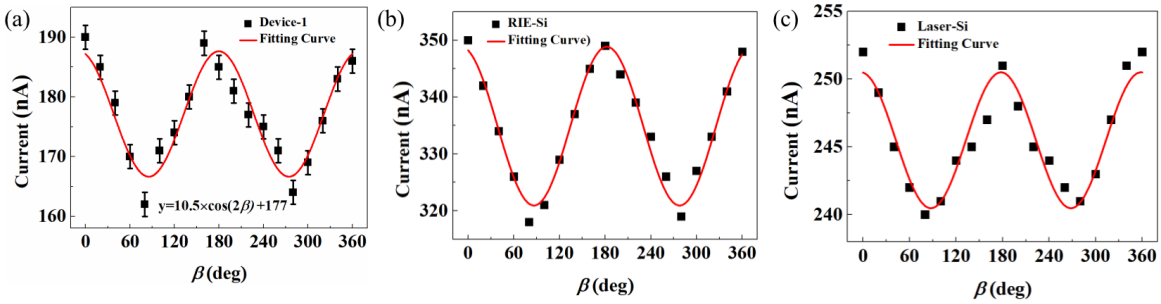

	Device-1	RIE-Si	Laser-Si
Extinction ratio	1.17	1.09	1.05

Fig. S7 (a) Polarization dependent photocurrent for the device with one spin, and that for the devices on the substrate etched by **(b)** reactive ion and **(c)** laser, respectively. The extinction ratio is summarized in the table.

Computation Section: Quantum transport simulations of the PGE photocurrent in the two-dimensional (2D) $Ti_3C_2T_x$ photodetector under the illumination of linearly polarized light at zero bias.

The $Ti_3C_2T_x$ photodetector contains several spins, which has multi-layers, and there are mismatch, distortion and overlapping between layers, which breaks the pristine space inversion symmetry of the 2D $Ti_3C_2T_x$. To mimic a $Ti_3C_2T_x$ photodetector, we use a bilayer $Ti_3C_2T_x$, as it is very time-consuming to use more layers for first-principles calculations. Figures S8(a) and (b) give top views of the F and OH

terminated $Ti_3C_2T_x$ surfaces, respectively. The red diamond part in the figure represents the primitive cell, where the Ti-F bond length is 2.197 Å and the Ti-O bond length is 2.202 Å [1].

The pristine bilayer Ti_3C_2 belongs to the D_{3d} symmetry, which has a space inversion symmetry and hence cannot produce the photogalvanic effect (PGE). Therefore, when constructing the device model for a photodetector, the top layer of the bilayer $Ti_3C_2T_x$ is displaced by 0.2 Å along the *z* axis to break the inversion symmetry. By this way, we mimic the broken space inversion symmetry by a mismatch or distortion in real device. The device model for the photodetector are shown in Figs. S8(c) and (d). The device contains the left and right electrodes, and a center region, which is irradiated by linearly polarized light, as indicated in Fig. S6(d). The entire model is periodic in the *x*-*z* plane, the *y* axis is the vacuum layer, the *x* axis is the zigzag direction, and the *z* axis is the armchair direction. The rectangular unit cell lattice constants of the bilayer Ti_3C_2 are a = 3.097 Å and c = 5.364 Å. We calculate the PGE photocurrent under the vertical illumination of linearly polarized light with the photon energies of 1.0, 1.165, and 2.0 eV.

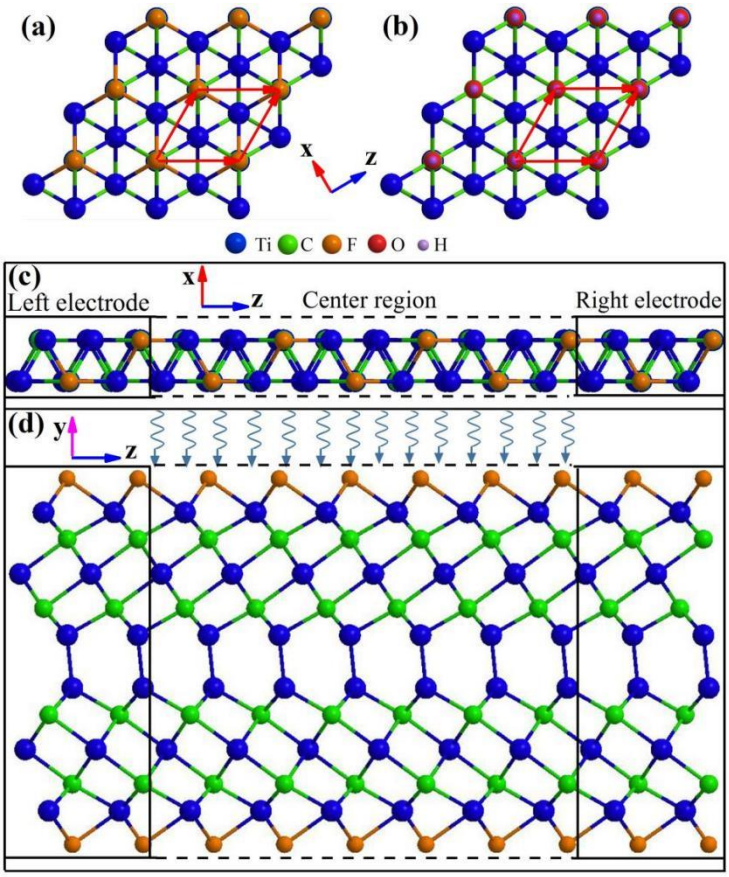

Fig. S8 Different passivation methods of bilayer Ti_3C_2: **(a)** -F, **(b)** -OH top view. The solid diamond-shaped red line represents the primitive cell. The blue, green, orange, red and purple spheres represent Ti, C, F, O and H atoms. The top view **(c)** and side view **(d)** of the bilayer Ti_2C_3 photoelectric detection model. The blue curved arrow in (d) represents linearly polarized light, which illuminates the entire central region.

The photocurrent is calculated using the first-principles quantum transport package Nanodcal [2], where density functional theory is used combined with nonequilibrium Green's formalism (NEGF-DFT). The photocurrent is calculated based on linear response theory [3]. Specifically, for linearly polarized light, the photocurrent injecting into the left lead (electrode) can be written as [4, 5]

$$J_L^{(ph)} = \frac{ie}{h}\int \{\cos^2\beta \mathrm{Tr}\{\Gamma_L[G_1^{<(ph)} + f_L(G_1^{>(ph)} - G_1^{<(ph)})]\}$$
$$+\sin^2\beta \mathrm{Tr}\{\Gamma_L[G_2^{<(ph)} + f_L(G_2^{>(ph)} - G_2^{<(ph)})]\}$$
$$+2\sin(2\beta)\mathrm{Tr}\{\Gamma_L[G_3^{<(ph)} + f_L(G_3^{>(ph)} - G_3^{<(ph)})]\}\}\mathrm{d}E,$$

where $G_{1,2,3}^{>/<(ph)}$ denotes the greater/lesser Green's functions with electron-photon interaction, which are determined by the symmetry, photon frequence and polarization

vector **e**. For linearly polarized light, the polarization vector **e** = cosβ**e**$_1$+ sinβ**e**$_2$, where β is the angle formed by the polarization direction with respect to the vector **e**$_1$. The vectors **e**$_1$ and **e**$_2$ are set along the zigzag and armchair directions, respectively. The photocurrent can be normalized as, $I_{ph} = J_L^{(ph)}/eI_\omega$ which still has dimensions of area of a_0^2/photon, where a_0 is the Bohr radius, and I_ω is photo flux. In the numerical calculations, the DZP atomic orbital basis is used to expand all the physical quantities; the exchange and correlation were treated at the level of the generalized gradient approximation (GGA) functional as parameterized by the PBE approximation; atomic cores are determined by the standard norm conserving nonlocal pseudopotentials, and 16×1×1 k-points are used. These calculation details are verified to obtain converged results.

References

1. Are MXenes promising anode materials for Li ion batteries? Computational studies on electronic properties and li storage capability of Ti_3C_2 and $Ti_3C_2X_2$ (X = F, OH) monolayer, *J. Am. Chem. Soc.* 134, 16909 (2012)
2. J. Taylor, H. Guo, and J. Wang, *Phys. Rev. B* 63, 245407 (2001)
3. L. E. Henrickson, J. Appl. Phys., 91, 6273 (2002)
4. Y. Xie, M. Chen, Z. Wu, Y. Hu, Y. Wang, J. Wang, and H. Guo, *Phys. Rev. Appl.* 10, 034005 (2018)
5. Y. Xie, L. Zhang, Y. Zhu, L. Liu, and H. Guo, *Nanotechnology* 26, 455202 (2015)